



Nanoscale

Computational screening of transition-metal single atoms doped C₉N₄ monolayer as efficient electrocatalysts for water splitting

Journal:	<i>Nanoscale</i>
Manuscript ID	NR-ART-07-2019-005991.R1
Article Type:	Paper
Date Submitted by the Author:	14-Aug-2019
Complete List of Authors:	Zhou, Yanan; Sichuan University, ; E O Lawrence Berkeley National Laboratory, Gao, Guoping; Lawrence Berkeley National Laboratory, Berkeley, Kang, Jun; Lawrence Berkeley National Laboratory, Materials Science Division Chu, Wei; Sichuan University, Chemical Engineering Department Wang, Lin-Wang; Lawrence Berkeley National Laboratory,

SCHOLARONE™
Manuscripts



Computational screening of transition-metal single atoms doped C₉N₄ monolayer as efficient electrocatalysts for water splitting

Yanan Zhou,^{ab} Guoping Gao,^b Jun Kang,^b Wei Chu,^{*a} and Lin-Wang Wang^{*b}

Received 00th January 20xx,
Accepted 00th January 20xx

DOI: 10.1039/x0xx00000x

www.rsc.org/

Searching for high efficiency and low-cost catalysts for the hydrogen evolution reaction (HER) and oxygen evolution reaction (OER) is vital to the overall water splitting. In this work, on the basis of first-principles calculations, we screened a series of late transition metal atoms supported on the C₉N₄ monolayer (TM@C₉N₄, where TM represents Mn, Fe, Co, Ni, Cu, Ru, Rh, Pd, Ir, and Pt) as electrocatalysts for both HER and OER. Our results demonstrate that the TM atoms can be bonded with the nitrogen atoms around the hole to form stable structures, and the bonded TM atoms are stable against diffusion. Co@C₉N₄ exhibits high catalytic activity toward HER. Especially, the N active sites in the Co@C₉N₄, Ni@C₉N₄, and Pt@C₉N₄ systems demonstrate relatively high performance for the HER. However, Co@C₉N₄ and Pt@C₉N₄ exhibit low OER activities with large overpotentials. Among the ten cases of TM@C₉N₄ considered here, only Ni@C₉N₄ performs as a promising bifunctional electrocatalyst with the N and Ni atoms as the catalytic active sites for the HER and OER, with the calculated hydrogen adsorption Gibbs free energy (ΔG_{H^*}) of -0.04 eV and OER overpotential (η^{OER}) of 0.31 V, respectively. The results demonstrate that TM@C₉N₄ is a promising single-atom catalytic system which can be used as the non-noble metal bifunctional electrocatalyst for overall water splitting.

Introduction

Hydrogen is expected to be an promising alternative clean energy source to traditional fossil fuels due to its high energy density and zero carbon emission in its usage.¹⁻³ Among many hydrogen production technologies, electrochemical water splitting has attracted enormous attention since it is a carbon neutral way to generate the hydrogen. The electrochemical water splitting involves two half-reactions: the cathodic hydrogen evolution reaction (HER) and anodic oxygen evolution reaction (OER). Up till now, the most advanced catalysts are Pt-based materials for HER,⁴ and Ru and Ir oxides for OER.⁵ However, high cost and scarcity of these noble metals

have limited their usage in large scale. Therefore, the development of high-efficiency and low-cost electrocatalysts without or less use of noble metal is of paramount importance.

Since the discovery of graphene,⁶ carbon-based materials have attracted numerous attention as promising catalysts for energy conversion. Notably, numerous efforts have been made in developing carbon-based catalysts for HER and OER due to their inherent conductivity, cost-effectiveness and wide use in electrochemistry.^{7,8} The activity of HER and OER can be significantly enhanced by introducing heteroatoms in graphene,^{7,9} or doping the two-dimensional (2D) material with transition metals.^{10,11} More importantly, carbon-based 2D materials exhibit great potential as promising substrates to disperse metal atoms as single-atom catalysts (SACs).¹² SACs can maximize the efficiency of metal atom use and provide tunable number of active sites. They have become a new frontier in catalysis research both experimentally and theoretically¹³ since the seminal work of Pt₁/FeO_x SAC reported by Zhang et al.¹⁴ However, due to the weak interaction between pure graphene and the transition metal, nitrogen atoms are

^a School of Chemical Engineering, Sichuan University, Chengdu, 610065, Sichuan, China

^b Materials Science Division, Lawrence Berkeley National Laboratory, Berkeley, 94720, California, United States

*E-mail address: chuwei1965@scu.edu.cn (Wei Chu); lwwang@lbl.gov (Lin-Wang Wang)

†Electronic Supplementary Information (ESI) available: See DOI: 10.1039/x0xx00000x

always introduced around the defect of graphene to enhance the binding strength to TM atoms. The catalytic activity of the TM and N codoped carbon/graphene for the water splitting has been investigated by the experiment^{7, 10, 15, 16} and theory.¹⁷⁻²² For instance, Tour et al²³ reported experimentally that very small amounts of Co dispersed as individual atoms on N doped graphene exhibits robust and high activity toward HER with very low overpotentials. Co-C₃N₄ catalyst possesses comparable electrocatalytic activity as the precious metal benchmarks for oxygen electrode reactions in the alkaline media.²⁴ Zhou et al²⁵ found that Mn1@C₂N could act as a promising bifunctional electrocatalyst toward HER and OER. All of these investigations manifest that the metal-nitrogen/carbon catalysts show high catalytic performance toward HER and OER.

All of the above investigations manifest that TM doped nitrogen/carbon systems show great potential as high performance catalyst for HER and OER processes. As more and more carbon nitride (CN) 2D systems are proposed and synthesized, it will be of great interests to identify the different types and mechanisms of using CN 2D systems as SAC substrate. Most previous studies involve introducing substitutional point defect to dope the CN 2D systems. This is either as TM and N codoped on graphene,^{20, 21, 26} or TM doping on a CN 2D system.^{25, 27} However, such doping might not always be easy to form high density of the sites, and the substitutional site size might not always be optimal. Another possibility which has not been fully explored is to simply attach a TM to the edge N atoms in an otherwise perfect CN 2D system. Here, we need to have edge N atoms in a CN 2D material, preferably for CN structures with relatively large pore with multiple N sites surrounding the pore. The attachment of TM on such N edge sites can thus be easily realized using electrochemical deposition. The site density can be as high as the number of pores. Fortunately, a new CN covalent 2D network with a C₉N₄ stoichiometry (shown in Fig. 1) was recently predicted theoretically by Niu et al,²⁸ which satisfies our requirement of having large pores with multiple edge N sites. The high thermodynamic and mechanical stabilities of C₉N₄ monolayer were confirmed by theoretical calculations.²⁸ Besides, compared to other experimental realizations of 2D carbonitrides, e.g., C₃N₄ and C₂N, first-principles calculations suggest that C₉N₄ monolayer exhibits nodal-line semi-metallic properties,²⁸ which is rather beneficial to be used as a catalytic electrode. This is different from other previously reported C-N compounds²⁹⁻³¹ and COFs,³² which are all semiconducting or insulation. The synthesis of C₉N₄ monolayer can be expected because theoretical prediction shows that it is energetically more stable than experimentally synthesized C₂N and g-C₃N₄.²⁸

All these salient features indicate that C₉N₄ monolayer could be a potential candidate as a substrate for anchoring single TM atom, and it is an ideal system for us to theoretically investigate the new mechanism of introducing TM atoms to the C₉N₄ substrate and their corresponding HER/OER performance.

Herein, we used first-principles calculations to systematically study the HER and OER catalytic performance of ten late TM atoms (Mn, Fe, Co, Ni, Cu, Ru, Rh, Pd, Ir, and Pt) doped on the C₉N₄ monolayer. These TM are chosen, as they have exhibited HER and OER activities in other 2D carbon-based materials.^{25, 33, 34} The Gibbs free energy change of adsorbed hydrogen (ΔG_{H^*}) was calculated to evaluate the HER catalytic activity. It is found that Co@C₉N₄ exhibits the highest catalytic performance toward HER. On the other hand, Ni@C₉N₄ exhibits the highest performance toward OER with an overpotential (η^{OER}) of 0.31 V. Overall, we found that Ni@C₉N₄ could act as a promising bifunctional HER and OER catalyst. All these suggest that C₉N₄ can be used as single-atom support for high performance catalysts for water splitting.

Computational methods

All the calculations were carried out at the spin-polarized density functional theory (DFT) level using the Vienna ab initio Simulation Package (VASP).³⁵ The generalized gradient approximation (GGA)³⁶ with the PerdewBurke-Ernzerhof (PBE) functional³⁷ and the projector augmented wave (PAW) pseudo-potentials³⁸ were used. The empirical correction method (DFT-D3)³⁹ was applied to describe the long-range van der Waals (vdW) effects. The electron wave-functions were expanded by plane-wave with cutoff energy of 500 eV, and the convergence criterion for energy and force during geometrical optimization was set to 10⁻⁵ eV and 10⁻² eV/Å, respectively. A vacuum space of 20 Å was used to avoid the interactions between periodic images. The Brillouin zones were sampled with 3x3x1 Monkhorst-Pack meshes.⁴⁰ The climbing image nudged elastic band (CINEB) method^{41, 42} was used to evaluate the diffusion barrier of the single atom among the nearest stable sites. To consider the effects of polarization due to the water, the polarizable implicit solvent model was used as implemented in VASPsol with the dielectric constant set to 78.4⁴³ during all the calculations. The details of HER and OER calculations are provided in the supporting information as in our previous work.²¹ The adsorption Gibbs free energy is defined as in the following equation (1):

$$G_{ads} = G_{adsorbent+catalyst} - G_{catalyst} - G_{adsorbent} \quad (1)$$

Here, $G_{adsorbent+catalyst}$, $G_{catalyst}$, and $G_{adsorbent}$ refer to the Gibbs free energy of adsorbent on catalyst, isolated catalyst, and isolated adsorbent, respectively.

Results and discussion

The optimized lattice parameter of the C_9N_4 unit cell is 9.63 Å, which agrees well with the literature.²⁸ A (2x2) supercell of the C_9N_4 containing 72 carbon atoms and 32 nitrogen atoms was used to model the C_9N_4 monolayer (Fig. 1a), and there exists a large hole surrounded by six nitrogen atoms. These atoms provide rich chemically active sites with lone pairs for TM connection. The geometry and stability of a single metal atom doped C_9N_4 monolayer was investigated. As shown in Fig. 1a, three possible anchoring sites were taken into consideration: i) the TM atom is adsorbed at the center of the holes (S1); ii) the TM atom connects with two N atoms (S2); or iii) the TM atom connects with three N atoms (S3). We optimized the three different adsorption configurations for the TM atoms to find the most energetically stable one. It is found that both of the S1 and S3 configurations will transform to the S2 configuration after optimization, indicating that S2 site is most preferred for the TM adsorption. The optimized stable structures are shown in Fig. S1. The adsorption energies between the TM atoms and the C_9N_4 monolayer were computed and shown in Fig. 1b. The large adsorption energies imply that the TM atoms could bond strongly with the C_9N_4 monolayer, instead of forming TM clusters, suggesting their good stabilities. As shown in Fig. 2, the strong hybridization between the p orbital of N and d orbital of TM atoms demonstrate the chemical bonding of N and TM atoms, which explains the strong interaction between TM and C_9N_4 monolayer. This is further

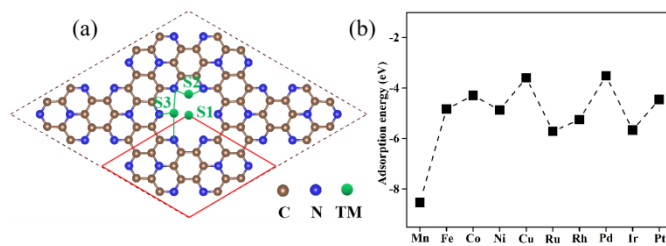


Fig. 1 (a) presents the (2x2) C_9N_4 supercell, where the red line indicates the unit cell, and different possible adsorption sites (S1, S2, and S3) for the single TM atoms doped on C_9N_4 monolayer. (b) Calculated adsorption energy of the corresponding TM@ C_9N_4 structure.

confirmed by the significant charge transfer from the TM atoms to the C_9N_4 monolayer (Table S3). Moreover, the diffusion possibility of the doped single atom (Ni@ C_9N_4 as an example) between the nearest stable sites was also calculated and shown in Fig. S2. Our result shows that the diffusion for the adsorbed Ni atoms needs to overcome a high energy barrier of 2.91 eV, which further suggests the stability of the TM atoms on C_9N_4 monolayer inhibits forming Ni diffusion. Efficient electrical conductivity could ensure the charge transfer of the catalyst for the HER and OER. Therefore, the density of states (DOS) of the TM@ C_9N_4 systems were computed to estimate the electrical conductivity and shown in Fig. S3. After doping TM atoms, all the TM@ C_9N_4 composites exhibit metallic properties, suggesting their good conductivities of the TM@ C_9N_4 composites which could further enhance the electrocatalytic performance.

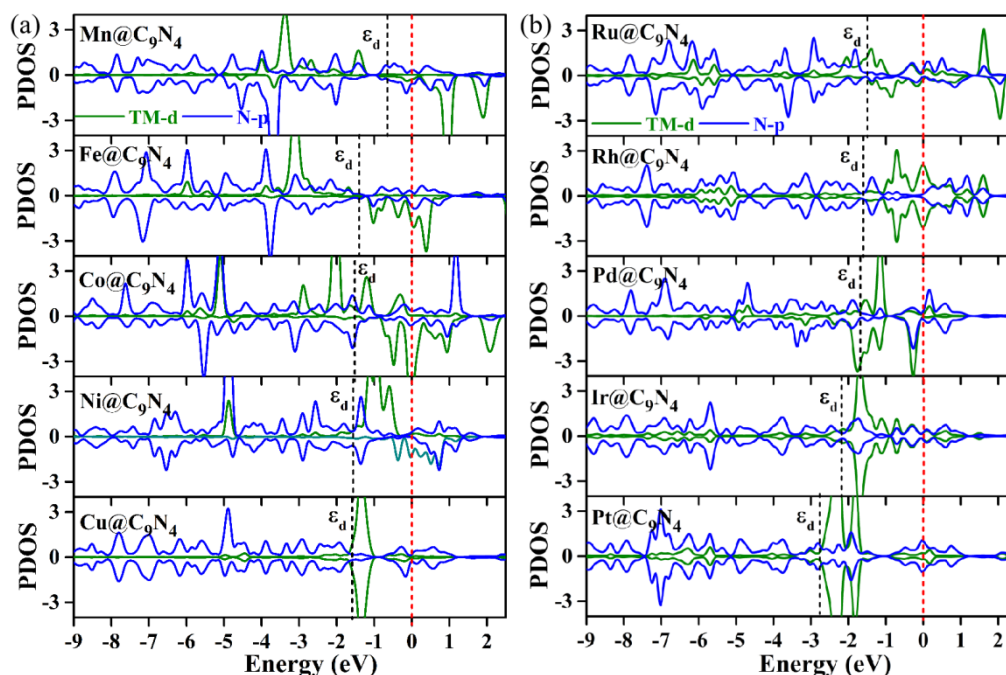


Fig. 2 Calculated PDOS illustrating the p orbital of N and the d orbital of TM atoms for considered TM@ C_9N_4 catalysts. The Fermi level is set at the zero highlighted by red dash line and the d band center (ϵ_d) is marked by the olive dash line.

The catalytic activities of the ten potential TM@C₉N₄ catalysts for the HER performance were investigated. The Gibbs free energy of adsorbed hydrogen on the catalyst (ΔG_{H^*}) is a vital descriptor to evaluate the HER activity of one catalyst. The Gibbs free energy value of an ideal catalyst should be close to zero eV, that's, $\Delta G_{H^*} \rightarrow 0$ eV. As defined above, a positive ΔG_{H^*} value of a catalyst indicates it is not kinetically favored for the hydrogen to adsorb on the catalyst. While, a catalyst with a negative ΔG_{H^*} value means it is difficult to release the adsorbed hydrogen on catalyst, thus restraining the HER activity. The calculated Gibbs free energy change for the hydrogen atom on the TM and the N atoms that bonded to the TM is presented in Fig. 3 and Table S4. The exchange current (i_0) can reflect the intrinsic rate of electrons in the HER at the equilibrium potential.⁴⁴ Thus, a volcano curve is plotted using exchange current i_0 as a function of the ΔG_{H^*} to compare the HER activity on the stable TM@C₉N₄ catalysts (Fig. 3a) and the computational details are shown in the supporting information. We can quantitatively evaluate the activity of HER from the position of the ΔG_{H^*} and i_0 with respect to the volcano peak. Closer the location of the value to the volcano peak, the better HER performance of the catalyst.⁴⁴ The ΔG_{H^*} for pristine C₉N₄ monolayer was also calculated for comparison. The value of ΔG_{H^*} for the N site on the pristine C₉N₄ is -1.03 eV, which suggests the strong interaction between the N and H atoms. Therefore, the pristine C₉N₄ monolayer is not a good catalyst for the HER. Interestingly, after TMs adsorbed on the C₉N₄ monolayer, the values of ΔG_{H^*} on the N atoms that bonded with TM (shown in Fig. S1) are changed. As we can see from Fig. 3b, the values of ΔG_{H^*} (N) for Co, Ni, and Pt catalysts are close to zero, thus they are located around the peak of the volcano curve with the maximum exchange current (Fig. 3a), suggesting that the N atoms in these systems (Co@C₉N₄, Ni@C₉N₄, and Pt@C₉N₄) could act as efficient sites for the HER. This change could be attributed to the charge

redistribution after TMs are doped on the C₉N₄. The N atoms gain about 1.15 e⁻ from C in the pristine C₉N₄ and the connected N atoms also obtain 1 e⁻ from the TMs in TM@C₉N₄ systems. Therefore, the value of ΔG_{H^*} increases, this trend agrees well with the previous results.²⁵ For the doped TM sites, the Co atom in Co@C₉N₄ could act as an efficient active site for HER. Remarkably, for Co@C₉N₄ catalyst, the ΔG_{H^*} for both the Co and N sites are close to the optimal value zero, indicating multiple active sites and good HER catalytic performance.

By studying the adsorption sites on the ten TM@C₉N₄ catalysts, it is found that the intermediates (HO*, O* and HOO*) prefer to be adsorbed on the top of the positively charged TM atoms. The detailed adsorption Gibbs free energies of adsorbed intermediates are summarized in Table S5. The Gibbs free energy differences of each reaction step for these TM@C₉N₄ systems were calculated to figure out the rate-determining step. The free energy diagrams for OER over the positively charged TM sites of the TM@C₉N₄ catalysts are shown in Fig. 4. As an ideal catalyst for OER, the energy barriers for all these steps (between two adjacent intermediate states) should be 1.23 eV. Thus, the OER overpotential (η^{OER}) is equal to 0 V and the OER can happen at its thermodynamic limit. While, in reality, the distance between two adjacent steps are not equal, and the η^{OER} is determined by the largest energy distance that labeled in blue. As we can see, the values of ΔG_{HO^*} for the first step of TM@C₉N₄ catalysts (TM = Mn, Fe, Co, and Ru) are all negative, from -0.02 to -0.21 eV, indicating the strong interaction between the catalysts and HO*. The third step that the formation of HOO* intermediate from the adsorbed O* intermediate or the fourth step that desorption of O₂ molecule from the catalyst surface becomes the rate-determining step. The calculated OER overpotentials for Mn, Fe, Co, and Ru are 0.87, 0.71, 0.88 and 1.11 V, respectively, indicating not so good OER catalytic efficiencies of them. The values of ΔG_{HO^*} for Ni@C₉N₄, Cu@C₉N₄,

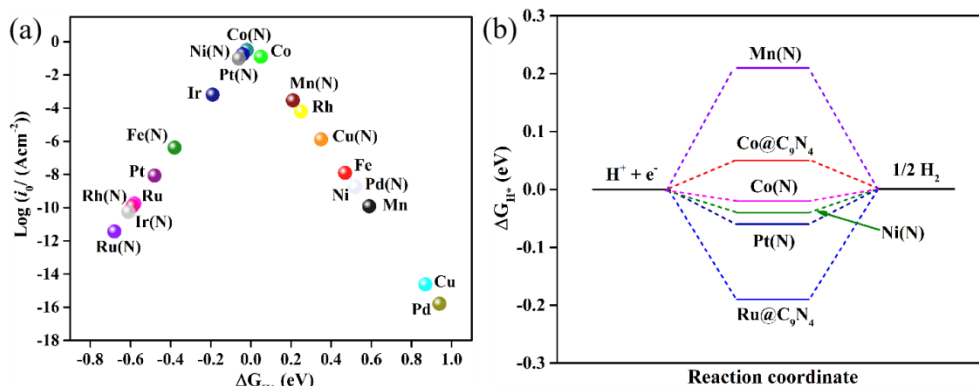


Fig. 3 (a) HER volcano curve of exchange current (i_0) related to the adsorption Gibbs free energy of hydrogen (ΔG_{H^*}) adsorbed on the different active sites of TM@C₉N₄ catalysts. (b) The calculated ΔG_{H^*} for the TM and N atoms in the TM@C₉N₄ catalysts.

and Rh@C₉N₄ systems are relatively positive, the second step, where the further dissociation of HO* to O*, is the potential-determining step with the calculated η being 0.31, 0.77 and 0.51 V, respectively. The calculated η for Cu@C₉N₄ is also too high to be used as efficient OER catalyst. For the remaining systems, the calculated η are 0.75, 0.93 and 0.78 V for Pd@C₉N₄, Ir@C₉N₄, and Pt@C₉N₄ composites, respectively, indicating they are also not the efficient catalysts for OER. Thus, to summarize, the best catalyst for the OER activity is Ni@C₉N₄ with an overpotential of 0.31 V. This is followed by Rh@C₉N₄ with a calculated η^{OER} of 0.51 V. The rate-determining steps for Ni@C₉N₄ and Rh@C₉N₄ are both found to be the formation of O* through HO* intermediate. The corresponding geometry structures for the Ni@C₉N₄ are shown in Fig. S4. The calculated

overpotential η^{OER} of Ni@C₉N₄ is close to or even lower than that of the well-studied Pt-based catalysts (about 0.4 V of PtO₂-rutile) for OER.⁴⁵ Therefore, we conclude that Ni@C₉N₄ is a promising candidate for OER, followed by the Rh@C₉N₄. Additionally, previous literature also reported that Ni-doped carbon materials could exhibit excellent OER performance.^{27, 34, 46}

Insights into the electronic structures of the considered different TM@C₉N₄ catalysts can guide us on how to improve the catalytic performance and design better catalysts. According to the Sabatier's principle,⁴⁴ too strong or too weak interaction between the doped active metal site and adsorbates will have negative effects on the catalytic performance. Too strong interaction could poison the electrode surface, while, too weak interaction could hinder the proton-

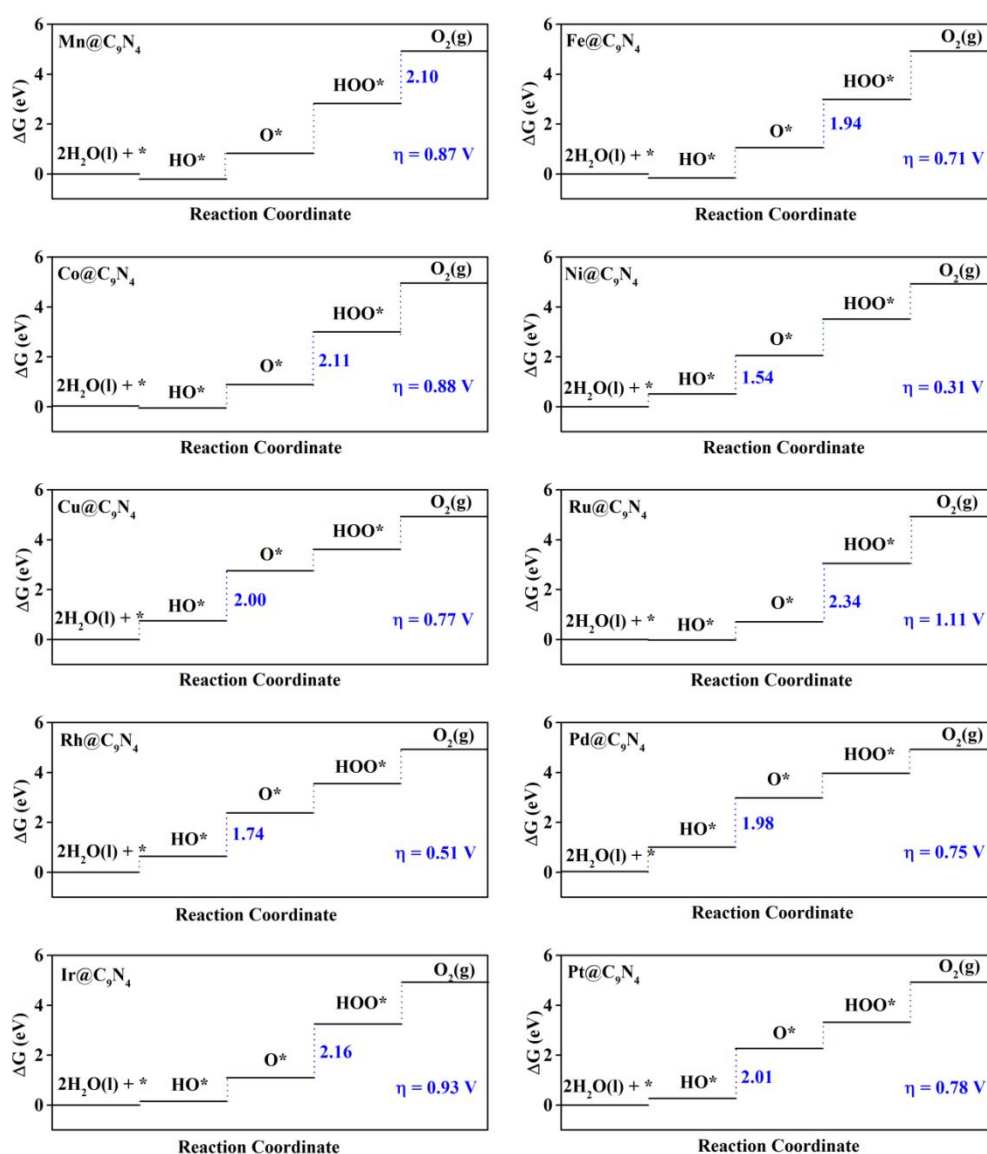


Fig. 4 Free energy diagram for OER on TM@C₉N₄ at the U = 0 V. The blue line is the rate-determining step for OER. The step (Gibbs free energy difference between two intermediate states) equals to $\Delta G_{a,b,c,d}$ of equation 5a~5d in the supporting information.

electron transfer for the intermediate.⁴⁷ Meanwhile, the d band center (ϵ_d) has been widely used to describe the interaction strength between adsorbate and substrate. Thus, we computed the d-orbitals of the doped TMs and obtained the d-band centers (shown in Fig. 2). As the number of d-electron of the anchored TMs increases, the d-band center moved to lower energy with respect to the Fermi level. Generally, the higher d-electron number and lower energy level of the d-band center will result in weaker interaction between the TMs and the intermediates.⁴⁸ It can be seen that there is a negative correlation between the d-band center and ΔG_{HO^*} when the TM atoms are in the same row (Fig. S5), which is in accordance with the above assumption. The strong interaction between the active sites and the intermediate usually results in high overpotentials of OER, such as the cases of Mn@C₉N₄, Fe@C₉N₄, and Co@C₉N₄ catalysts.

It is customary to find a relationship between three adsorbed intermediates Gibbs free energy (ΔG_{O^*} , ΔG_{HO^*} and ΔG_{HOO^*}), and then use them to construct a descriptor to describe the OER performance.⁴⁹ By comparing the adsorption Gibbs free energy of HO* and HOO* for the wide range of TMs doped C₉N₄, we found that ΔG_{HOO^*} can be expressed as a function of ΔG_{HO^*} via equation by $\Delta G_{\text{HOO}^*} = 0.84\Delta G_{\text{HO}^*} + 3.07$ eV as shown in Fig. 5a. The coefficient of determination (R^2) is 0.973, indicating that the linear relationship between HO* and HOO* is strong. This result is consistent with the previous studies of carbon-based materials for OER.^{21, 33, 50, 51} The close to 1 slope between HO* and HOO* implies that both these two intermediates (HO* and HOO*) have a single bond between an O atom and the TM. Note that, if we assume the slope of the above equation is 1, it implies that the difference between ΔG_{HOO^*} and ΔG_{HO^*} ($\Delta G_{\text{HOO}^*} - \Delta G_{\text{HO}^*}$) should be constant. Since all the rate-determining steps for OER happen either at the step of O* formation or the HOO* formation (with the

exception of Mn, where its O* to HOO* step distance is almost same as the HOO* to O₂ distance), then the OER overpotential will be determined by the distance of $\Delta G_{\text{O}^*} - \Delta G_{\text{HO}^*}$. This is confirmed by the volcano plot shown in Fig. 5b. Note the dashed line in Fig. 5b is obtained using assumption that $\Delta G_{\text{HOO}^*} - \Delta G_{\text{HO}^*}$ is a constant. The smallest overpotential among the considered catalysts occurs around Ni@C₉N₄, when its $\Delta G_{\text{O}^*} - \Delta G_{\text{HO}^*}$ is close to a half of $\Delta G_{\text{HOO}^*} - \Delta G_{\text{HO}^*}$.

Conclusions

In summary, we have investigated a large number of transition metal atoms doped C₉N₄ composites for the HER and OER by computational screening approach. Compared to defect induced TM doping, such system will have more sites for TM adsorption, thus can have higher efficiency for catalysis. Our results show that the interaction strength between all the considered TM single atoms and C₉N₄ monolayer are strong. The barrier of diffusion of the doped TMs from its stable adsorption site to the neighboring site is high, making them exhibits relatively high activity for HER performance, and it is the N atoms act as the active sites in Co@C₉N₄, Ni@C₉N₄, and Pt@C₉N₄ systems. We have also evaluated the OER activity of these catalysts by computing their OER overpotentials. It is found that Ni@C₉N₄ is the best catalyst for OER with η^{OER} of 0.31 V, followed by Rh@C₉N₄ (0.51 V). Therefore, Ni@C₉N₄ could be a promising bifunctional electrocatalyst for overall water splitting, in which Ni atom act as the catalytic active site for OER with the lowest overpotential of 0.31 V, and N atoms perform the active site for HER with ΔG_{H^*} of -0.04 V. Overall, our calculated results highlight a promising 2D material substrate which can be used to design efficient non-precious metal HER/OER catalysts and offer a novel strategy to select the optimal active catalytic sites in other carbon-based materials.

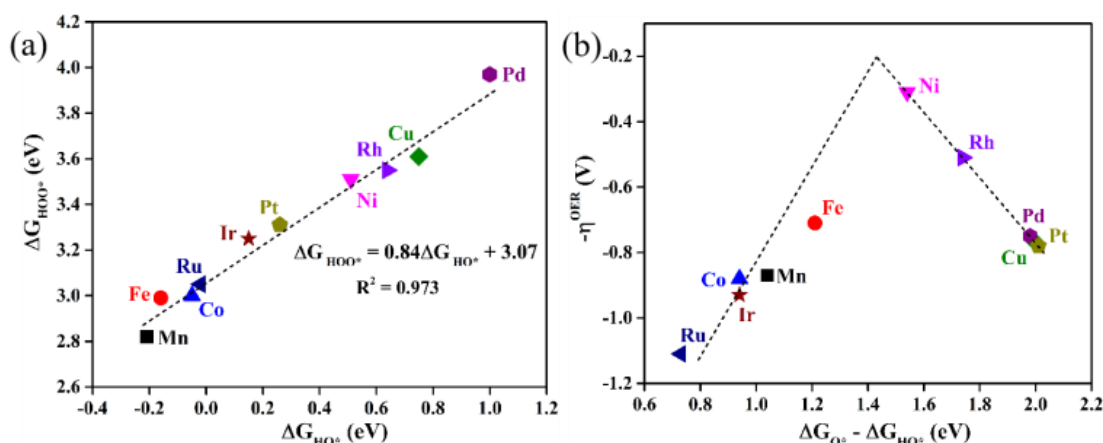


Fig. 5 (a) Scaling relationship between ΔG_{HO^*} and ΔG_{HOO^*} on TM@C₉N₄, (b) the calculated negative overpotential ($-\eta^{\text{OER}}$) against $\Delta G_{\text{O}^*} - \Delta G_{\text{HO}^*}$ on TM@C₉N₄.

Conflicts of interest

There are no conflicts to declare.

Acknowledgements

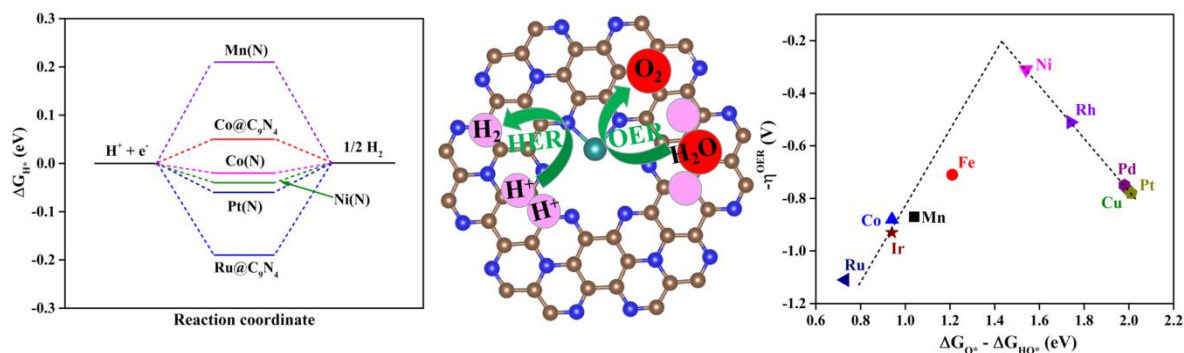
This work was supported by the Assistant Secretary for Energy Efficiency and Renewal Energy of the U.S. Department of Energy under the Hydrogen Generation program. This theoretical work used the resources of the National Energy Research Scientific Computing Center (NERSC) that is supported by the Office of Science of the U. S. Department of Energy. We are grateful to the Chinese Scholarship Council (CSC) for providing the Ph.D. scholarship and to Lawrence Berkeley National Laboratory (United States) for financial support.

References

1. J. A. Turner, *Science.*, 2004, **305**, 972–974.
2. M. Balat, *Int. J. Hydrogen. Energ.*, 2008, **33**, 4013–4029.
3. S. Chu and A. Majumdar, *Nature.*, 2012, **488**, 294–303.
4. M. G. Walter, E. L. Warren, J. R. McKone, S. W. Boettcher, Q. Mi, E. A. Santori and N. S. Lewis, *Chem. Rev.*, 2010, **110**, 6446–6473.
5. Y. Lee, J. Suntivich, K. J. May, E. E. Perry and Y. Shao-Horn, *J. Phys. Chem. Lett.*, 2012, **3**, 399–404.
6. K. S. Novoselov, A. K. Geim, S. V. Morozov, D. Jiang, Y. Zhang, S. V. Dubonos, I. V. Grigorieva and A. A. Firsov, *Science.*, 2004, **306**, 666–669.
7. L. L. Zhang, J. Xiao, H. Y. Wang and M. H. Shao, *ACS. Catal.*, 2017, **7**, 7855–7865.
8. C. L. Tan, X. H. Cao, X. J. Wu, Q. Y. He, J. Yang, X. Zhang, J. Z. Chen, W. Zhao, S. K. Han, G. H. Nam, M. Sindoro and H. Zhang, *Chem. Rev.*, 2017, **117**, 6225–6331.
9. J. T. Zhang, Z. H. Zhao, Z. H. Xia and L. M. Dai, *Nat. Nanotechnol.*, 2015, **10**, 444–452.
10. C. Z. Zhu, Q. R. Shi, S. Feng, D. Du and Y. H. Lin, *ACS. Energy. Lett.*, 2018, **3**, 1713–1721.
11. Y. P. Zhu, C. X. Guo, Y. Zheng and S. Z. Qiao, *Acc. Chem. Res.*, 2017, **50**, 915–923.
12. B. Bayatsarmadi, Y. Zheng, A. Vasileff and S. Z. Qiao, *Small.*, 2017, **13**, 1700191.
13. X. F. Yang, A. Q. Wang, B. T. Qiao, J. Li, J. Y. Liu and T. Zhang, *Acc. Chem. Res.*, 2013, **46**, 1740–1748.
14. B. T. Qiao, A. Q. Wang, X. F. Yang, L. F. Allard, Z. Jiang, Y. T. Cui, J. Y. Liu, J. Li and T. Zhang, *Nat. Chem.*, 2011, **3**, 634–641.
15. P. Z. Chen, T. P. Zhou, L. L. Xing, K. Xu, Y. Tong, H. Xie, L. D. Zhang, W. S. Yan, W. S. Chu, C. Z. Wu and Y. Xie, *Angew. Chem. Int. Ed.*, 2017, **56**, 610–614.
16. J. Li and G. F. Zheng, *Angew. Adv. Sci.*, 2017, **4**, 1600380.
17. X. L. Zhang, Z. X. Yang, Z. S. Lu and W. C. Wang, *Carbon.*, 2018, **130**, 112–119.
18. Y. Jiao, Y. Zheng, M. Jaroniec and S. Z. Qiao, *Chem. Soc. Rev.*, 2015, **44**, 2060–2086.
19. G. P. Gao, S. Bottle and A. J. Du, *Catal. Sci. Technol.*, 2018, **8**, 996–1001.
20. X. P. Gao, Y. N. Zhou, Y. J. Tan, B. W. Yang, Z. W. Cheng, Z. M. Shen and J. P. Jia, *Appl. Surf. Sci.*, 2019, **473**, 770–776.
21. Y. N. Zhou, G. P. Gao, Y. Li, W. Chu and L. L. Wang, *Phys. Chem. Chem. Phys.*, 2019, **21**, 3024–3032.
22. Y. N. Zhou, G. P. Gao, J. Kang, W. Chu and L. L. Wang, *J. Mater. Chem. A.*, 2019, **7**, 12050–12059.
23. H. L. Fei, J. C. Dong, M. J. Arellano-Jimenez, G. L. Ye, N. D. Kim, E. L. G. Samuel, Z. W. Peng, Z. Zhu, F. Qin, J. M. Bao, M. J. Yacaman, P. M. Ajayan, D. L. Chen and J.M. Tour, *Nat. Commun.*, 2015, **6**, 8668.
24. Y. Zheng, Y. Jiao, Y. H. Zhu, Q. R. Cai, A. Vasileff, L. H. Li, Y. Han, Y. Chen and S. Z. Qiao, *J. Am. Chem. Soc.*, 2017, **139**, 3336–3339.
25. X. Zhang, A. Chen, Z. H. Zhang, M. G. Jiao and Z. Zhou, *J. Mater. Chem. A.*, 2018, **6**, 11446–11452.
26. X. Liu, Y. Jiao, Y. Zheng, K. Davey and S. Z. Qiao, *J. Mater. Chem. A.*, 2019, **7**, 3648–3654.
27. X. Y. Li, P. Cui, W. H. Zhong, J. Li, X. J. Wang, Z. W. Wang and J. Jiang, *Chem. Commun.*, 2016, **52**, 13233–13236.
28. H. Y. Chen, S. H. Zhang, W. Jiang, C. X. Zhang, H. Guo, Z. Liu, Z. M. Wang, F. Liu and X. B. Niu, *J. Mater. Chem. A.*, 2018, **6**, 11252–11259.
29. J. Mahmood, E. K. Lee, M. Jung, D. B. Shin, H. J. Choi, J. M. Seo, S. M. Jung, D. Kim, F. Li, M. S. Lah, N. Park, H. J. Shin, J. H. Oh and J. B. Baek, *PNAS.*, 2016, **113**, 7414–7419.
30. X. C. Wang, K. Maeda, A. Thomas, K. Takanabe, G. Xin, J. M. Carlsson, K. Domen and M. Antonietti, *Nat. Mater.*, 2009, **8**, 76–80.
31. J. Mahmood, E. K. Lee, M. Jung, D. B. Shin, I. Y. Jeon, S. M. Jung, H. J. Choi, J. M. Seo, S. Y. Bae, S. D. Sohn, N. Park, J. H. Oh, H. J. Shin and J. B. Baek, *Nat. Commun.*, 2015, **6**, 6486.
32. C. S. Diercks and O. M. Yaghi, *Science.*, 2017, **355**, 923–931
33. G. P. Gao, E. R. Waclawik and A. J. Du, *J. Catal.*, 2017, **352**, 579–585.
34. T. W. He, S. K. Matta, G. Will and A. J. Du, *Small. Methods.*, 2019, **352**, 1800419.
35. G. Kresse and J. Furthmuller, *Comp. Mater. Sci.*, 1996, **6**, 15–50.
36. J. P. Perdew, K. Burke and M. Ernzerhof, *Phys. Rev. Lett.*, 1996, **77**, 3865–3868.
37. J. P. Perdew, M. Ernzerhof and K. Burke, *J. Chem. Phys.*, 1996, **105**, 9982–9985.
38. P. E. Blöchl, *Phys. Rev. B: Condens. Matter Mater. Phys.*, 1994, **50**, 17953–17979.
39. S. Grimme, J. Antony, S. Ehrlich and H. Krieg, *J. Chem. Phys.*, 2010, **132**, 154104–154123.
40. H. J. Monkhorst and J. D. Pack, *Phys. Rev. B.*, 1976, **13**, 5188–5192.
41. G. Henkelman, B. P. Uberuaga and H. Jonsson, *J. Chem. Phys.*, 2000, **113**, 9901–9904.
42. G. Henkelman, A. Arnaldsson and H. Jonsson, *Comput. Mater. Sci.*, 2006, **36**, 354–360.
43. K. Mathew, R. Sundararaman, K. Letchworth-Weaver, T. A. Arias and R. G. Hennig, *J. Chem. Phys.*, 2014, **140**, 084106–084114.
44. J. K. Nørskov, T. Bligaard, A. Logadottir, J. R. Kitchin, J. G. Chen, S. Pandalov and U. Stimming, *J. Electrochem. Soc.*, 2005, **152**, J23–J26.
45. J. K. Nørskov, J. Rossmeisl, A. Logadottir and L. Lindqvist, *J. Phys. Chem. B.*, 2004, **108**, 17886–17892.
46. F. L. Wang, G. Chen, X. H. Liu, F. S. Chen, H. Wan, L. S. Ni, N. Zhang, R. Z. Ma and G. Z. Qiu, *ACS. Sustainable. Chem. Eng.*, 2018, **7**, 341–349.
47. C. Y. Ling, L. Shi, Y. X. Ouyang, X. C. Zeng and J. L. Wang, *Nano. Lett.*, 2017, **17**, 5133–5139.
48. F. Calle-Vallejo, A. Krabbe and J. M. Garcia-Lastra, *Chem. Sci.*, 2017, **8**, 124–130.
49. M. T. M. Koper, *J. Electroanal. Chem.*, 2011, **660**, 254–260.
50. H. X. Xu, D. J. Cheng, D. P. Cao and X. C. Zeng, *Nat. Catal.*, 2018, **1**, 339–348.

51. S. Zhou, N. S. Liu, Z. Y. Wang and J. J. Zhao, *ACS. Appl. Mater. Interfaces.*, 2017, **9**, 22578-22587.

Graphical abstract



Ni@C₉N₄ performs as a promising bifunctional electrocatalyst with the N and Ni atoms as the catalytic active sites for the HER and OER, with the calculated hydrogen adsorption Gibbs free energy (ΔG_{H^*}) of -0.04 eV and OER overpotential (η^{OER}) of 0.31 V, respectively.